JOURNAL OF PROPULSION AND POWER
Vol. 27, No. 1, January–February 2011

Electron Backstreaming Determination for Ion Thrusters

Richard E. Wirz*
University of California, Los Angeles, Los Angeles, California 90095
and
Ira Katz,† Dan M. Goebel,‡ and John R. Anderson§
Jet Propulsion Laboratory, California Institute of Technology, Pasadena, California 91001

DOI: 10.2514/1.46844

Electron backstreaming in ion thrusters is caused by the random flux of beam electrons past a potential barrier established by the accelerator grid. A technique that integrates this flux over the radial extent of the barrier reveals important aspects of electron backstreaming phenomena for individual beamlets, across the thruster beam, and throughout thruster life. For individual beamlets it was found that over 99% of the electron backstreaming occurs in a small area at the center of the beamlet that is less than 20% the area of the beamlet at the potential barrier established by the accelerator grid. For the thruster beam it was found that over 99% of the backstreaming current occurs inside of $r = 6$ cm for the over 28 cm diameter NSTAR grid. Initial validation against extended life test data for the NSTAR thruster shows that the technique provides the correct behavior and magnitude of electron backstreaming limit, $|V_{ebs}|$. From the sensitivity analyses it is apparent that accelerator grid chamfering due to sputter erosion contributes significantly to the sharp rise in electron backstreaming limit observed in the extended life test, but does not explain the rise in grid ion transparency. Reduction of the grid gap over the life of the thruster also contributes to increases in electron backstreaming limit and increases in ion transparency. Screen grid erosion contributes generally to rises in $|V_{ebs}|$ and grid ion transparency, but for the assumptions used herein, it appears to not have as much of an effect as chamfering or grid gap change. Overall, it is apparent that accelerator grid chamfering, grid gap change, and screen grid erosion are important to the increase in electron backstreaming observed during the NSTAR extended life test.

Nomenclature

$\bar{c}$	=	average thermal speed
e	=	electron charge
f_{ebs}	=	electron backstreaming fraction
I_{ebs}	=	electron backstreaming current
I_i	=	ion current
n_{bp}	=	average downstream beamlet plasma density
n_e	=	electron density
r	=	radius
r_{max}	=	maximum radius of the accelerator grid aperture
T_e	=	electron temperature
V_{ebs}	=	electron backstreaming limit
Γ_e	=	electron flux
ϕ	=	local potential
ϕ_{bp}	=	beam potential
ϕ_m	=	minimum potential along for a radial distance from beamlet axis

I. Introduction

ELECTRON backstreaming in ion thrusters is caused by beam electrons that have sufficient energy to exceed the potential barrier established by the accelerator grid and can thus flow into the discharge chamber. A schematic of this potential barrier is shown in Fig. 1, which shows approximate axial potential traces at differing radial positions in the beamlet. Excessive electron backstreaming reduces thruster efficiency and life; therefore, an electron backstreaming fraction f_{ebs}, limit of 1% for the entire thruster beam [where f_{ebs} is defined in Eq. (1) below] is used in this study, which is similar to electron backstreaming criteria used in experimental efforts for ion thrusters. The minimum accelerator grid voltage required to keep f_{ebs} below 1% is called the electron backstreaming limit V_{ebs}. For this condition, the Deep Space One flight spare ion thruster used for the extended life test (ELT) lost the ability to run at full power (TH15) after processing 211 kg of xenon propellant due to an electron backstreaming limit that exceeded the capability of the accelerator grid power supply [1].

Electron backstreaming was first analyzed by Kaufman [2]. For grids sets with large grid gap compared with the accelerator grid hole diameter, and neglecting the beam space charge, he developed an analytical expression for the electron backstreaming limit V_{ebs}, based on grid voltages and macroscopic grid dimensions. Nakano and Arakawa [3] and Nakano [4] later developed a method that assumes that thruster end-of-life (EOL) occurs when the *saddle point* voltage on the beamlet axis reaches 0 V. Williams et al. [5] used the concept of the axial saddle point to develop an analytical expression that predicts the electron backstreaming current for a single beamlet as a function of ion beamlet current, macroscopic grid dimensions, ion mass, and downstream electron temperature. This method (referred to as the WGW method herein) accounts for many important contributors to electron backstreaming. Using inputs from multiple NSTAR thruster tests, the WGW model was used as part of a prelaunch investigation of the estimated life of the NSTAR thrusters currently being used the DAWN mission [1]. From this investigation it is apparent that the WGW model is a useful tool provided sufficient information about the thruster is known; however, it is very sensitive to the beamlet diameter and grid dimensions, and so provides only an estimate of the values. Similar to Kaufmann's model, the WGW model is only appropriate for grids where the grid gap is much larger than the accelerator grid hole diameter, a geometry that is not commonly used in modern grid design. Additionally, the Kaufmann

Presented as Paper 2008-4732 at the 44th AIAA/ASME/SAE/ASEE Joint Propulsion Conference and Exhibit, Hartford, CT, 21–23 July 2008; received 24 August 2009; revision received 15 March 2010; accepted for publication 17 June 2010.

*Assistant Professor, Mechanical and Aerospace Engineering, 420 Westwood Plaza, Eng. IV 46-147B; wirz@ucla.edu.
†Group Supervisor, Electric Propulsion Group, 4800 Oak Grove, M-S 125-109.
‡Senior Research Scientist, Propulsion and Materials Engineering Section, 4800 Oak Grove, M-S 125-109.
§Senior Engineer, Electric Propulsion Group, 4800 Oak Grove, M-S 125-109.

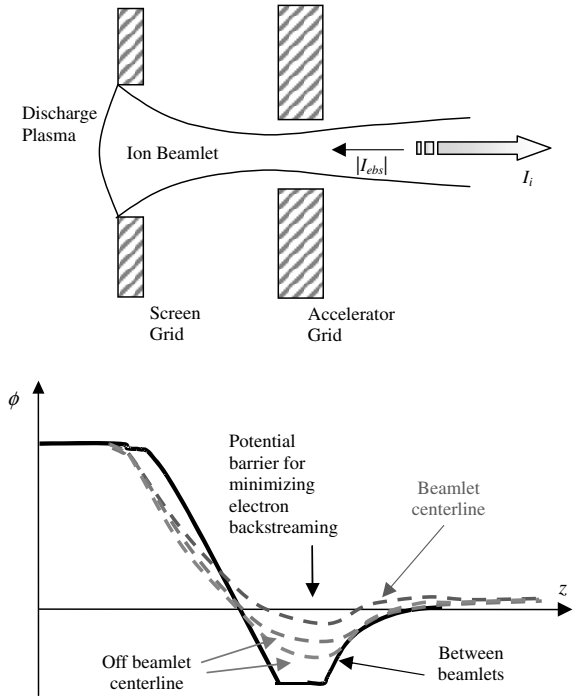

Fig. 1 Schematic of a gridlet and a plot of approximate beamlet potential as a function of axial location at various radial positions from beamlet axis.

and WGW models assume simple cylindrical aperture geometries and can thus not account for noncylindrical grid geometries such as cusps and geometric details due to grid erosion.

As discussed below, electron backstreaming occurs over the entire beamlet and therefore a rigorous treatment that accounts for the radial variation of retarding potential and electron flux is required. The objective of this investigation is to present a new and more rigorous electron backstreaming model that uses computational results of the radial and axial variations of potentials at the potential barrier for grid apertures of any shape. This new technique allows the treatment of detailed grid geometries, such as those generated during grid erosion, and can therefore be used for accurate determination of electron backstreaming as the grids erode over the life of the thruster.

II. Technique and Formulation

Electron backstreaming is caused by the random flux of high-energy electrons past the potential barrier established by the accelerator grid. The high-energy electrons come from the tail of the thermal distribution of beam electrons. The retarding potential (the minimum potential measured along the direction of the beamlet axis) varies radially in the beamlet, resulting in a predominately radial dependence of electron backstreaming within a given beamlet. The formulation below provides a technique that can be used with ion optics codes that compute the potential values for a beamlet. This technique also works with codes, such as CEX2D-t, which provide a detailed eroded geometry of the grids using time-dependent erosion as discussed in reference [6].

The backstreaming fraction f_{ebs} for a beamlet or the entire beam is the ratio of backstreaming electron current I_{ebs} to the outgoing ion current I_i, through an individual gridlet (herein, a *gridlet* is a single set of gird apertures as pictured in Fig. 1) or the entire grid surface, depending on the domain of the problem, such that

$$f_{\text{ebs}} \equiv \frac{I_{\text{ebs}}}{I_i} \tag{1}$$

Several ion optics codes calculate the ion current, I_i, for a single beamlet for given plasma and thruster operating conditions. These codes also compute the plasma potentials throughout the computational domain. With this information, the electron backstreaming can be estimated by considering the electron momentum. In the beamlet region one can assume the electrons are nearly in thermal equilibrium; in addition the electron drift, inertial, magnetic, and frictional forces are negligible such that the electron density n_e at a local potential ϕ can be described by Boltzmann's relation

$$n_e = n_{\text{bp}} \exp\left[\frac{\phi - \phi_{\text{bp}}}{T_e}\right] \tag{2}$$

where n_{bp} is the average downstream beamlet density at the beam potential ϕ_{bp}. For ion thrusters, the accelerator grid sets up a potential barrier in the beamlet to prevent prodigious backstreaming of beam electrons. The flux of backstreaming electrons from the beam across a local potential minimum ϕ_m that will make it back into the discharge chamber can be determined by using the Boltzmann relation to determine the electron density at the location of a minimum potential as a function of the downstream beam plasma potential ϕ_{bp} and the beam plasma density n_{bp}. Therefore, the one-sided thermal flux of electrons is

$$\Gamma_e = \frac{n_{\text{bp}}\bar{c}}{4} \exp\left[\frac{\phi_m - \phi_{\text{bp}}}{T_e}\right] \tag{3}$$

where $\bar{c}$ is the average thermal speed of the beam electrons at temperature T_e. The radial locus of local minimum potentials created by the accelerator grid typically resides nearly along the upstream end of the accelerator grid. Therefore, the electron backstreaming flux can be considered radially dependent such that

$$\Gamma_e(r) = \frac{n_{\text{bp}}\bar{c}}{4} \exp\left[\frac{\phi_m(r) - \phi_{\text{bp}}}{T_e}\right] \tag{4}$$

The electron backstreaming current for a beamlet is then given by integrating over the beamlet along the local minimum potentials

$$\begin{aligned} I_{\text{ebs}} &= e2\pi \int_0^{r_{\max}} \Gamma_e(r) r \, \mathrm{d}r \\ &= e\left(\frac{n_{\text{bp}}\bar{c}}{4}\right) 2\pi \int_0^{r_{\max}} \exp\left[\frac{\phi_m(r) - \phi_{\text{bp}}}{T_e}\right] r \, \mathrm{d}r \end{aligned} \tag{5}$$

where $r_{\max}$ is the minimum diameter of the accelerator grid aperture, and hence the maximum radius for electron backstreaming to the discharge chamber. For a computational implementation of this result, one may adjust the flux area based on the relative axial locations of ϕ_m for discrete radial locations; however, this was not found to be important for the cases examined herein.

The ion optics code models the electron space-charge density by barometric law and assumes that the electrons are Maxwellian in the discharge chamber and in the beam downstream of the thruster. The temperatures of the electrons in these regions are specified separately by the user. The potentials between these regions (i.e., between the grids) are dominated by the boundary conditions established by the potential applied to the grid surfaces; therefore, the space charge effects of the backstreaming electrons will be minimal. Additionally, during nominal operation of the thruster the backstreaming electron density will be at least an order of magnitude less than the ion density, thus minimizing the relative space charge effects of backstreaming electrons in this region.

III. Results

The formulation from Sec. II is used in this section to examine the electron backstreaming for individual gridlets and across the beam of the NSTAR. These tools are also used to investigate the electron backstreaming behavior observed during the ELT.

A. Inputs and Gridlet Potential Solutions

Posttest analysis of the NSTAR thrusters at the conclusion of the LDT and ELT tests showed that the center region of the grids experienced the most erosion and accelerator grid aperture enlargement, features which lead to increased electron backstreaming [1,7]. This worst-case erosion was simulated in [6] for the full duration of

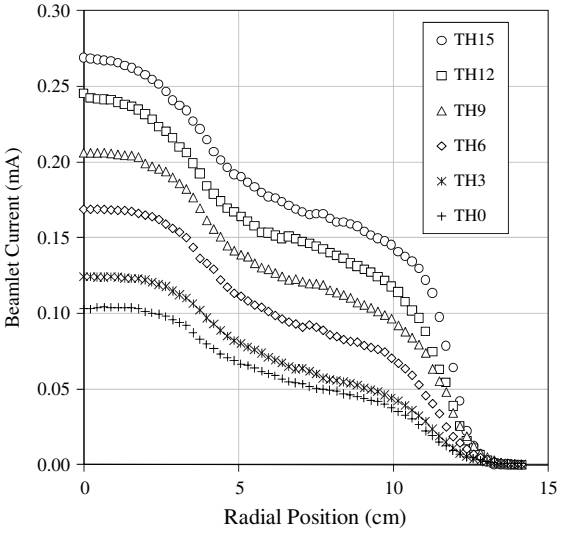

Fig. 2 Beamlet current vs radial position for LDT at TH15 and ELT for various throttle conditions.

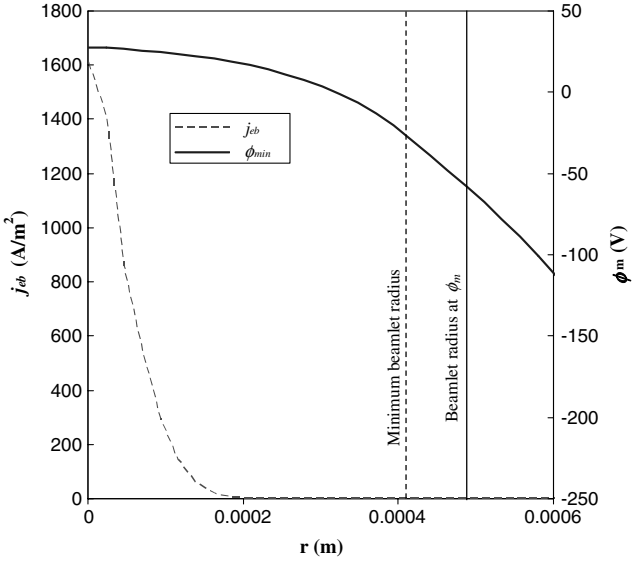

Fig. 3 Electron backstreaming current density j_{eb} and minimum potential ϕ_m, vs beamlet radius for TH15 at ELT EOL condition for center beamlet. (Note: the minimum beamlet radius is typically found just upstream of the accelerator grid while the minimum potential is typically just downstream of the accelerator grid.)

the ELT. In this investigation we use the results from these simulations, as discussed below, to provide the accelerator grid chamfer angles for sensitivity and validation efforts. The potential for the downstream beam plasma ϕ_{bp} and electron temperature T_e were taken as 15 V and 1.8 eV, respectively, as discussed in [1]. The upstream electron temperature used was 5 eV and the neutral densities for TH15 were taken as the average of the neutral density from the exit plane neutral profiles in [8].

The mean hot grid gap (during thruster operation) used for the center hole at BOL was the 0.30 mm spacing measured for TH15 in [9] (this assumes an initial cold grid gap of 0.66 mm and a lessening of the grid gap by 0.36 mm during thruster operation). Per [9], the uncertainty in grid gap during these measurements was approximately ± 0.01 mm for the high power throttle condition (TH15) and $+0.02/-0.01$ mm for the midpower condition (TH8). Because data on the radial variation of the hot grid gap is unavailable, this study assumes that the hot grid gap varies linearly from 0.30 mm at the center grid to 0.66 mm at the grid periphery at BOL. Posttest analysis for the ELT showed that the cold grid gap had changed approximately -0.19 mm. Therefore, the EOL minimum hot grid gap was assumed to vary linearly from 0.11 mm at the center grid to 0.47 mm at the grid periphery at BOL. Sensitivity analyses given below show that reduction of hot grid gap on this order help to explain sharp rises in the magnitude of the electron backstreaming at the end of life. The NSTAR grid dimensions have been previously been reported in several papers, including [10].

The potential fields for the beamlets are determined by CEX2D, which is described in detail in [11]. To determine the electron backstreaming limit V_{ebs} for each case the accelerator grid voltage is swept through a range of voltages to find the point at which the backstreaming condition of $f_{ebs} = 1\%$ for the entire beam is achieved (similar to the method used to experimentally determine V_{ebs}) using the formulation from Sec. II.

B. Electron Backstreaming Integration over Single Gridlets and Thruster Grid Profiles

Electron backstreaming (EBS) was determined for the NSTAR profiles shown in Fig. 2, for which the beamlet currents were calculated from ELT Faraday probe traces using the technique discussed in [1]. Using these beamlet densities and the formulation from Sec. II, it was found that the potential barrier is essentially just upstream of the accelerator grid for most configurations. After integrating Eq. (5) over this potential barrier for several single beamlets it was found that over 99% of the electron backstreaming occurs in a small area that is less than 20% the size of the beamlet at this location. This concentration of electron backstreaming current can be seen from plots of the electron backstreaming current density versus beamlet radius, as shown in Fig. 3. This plot is indicative of the electron backstreaming current distribution in the beamlet for all conditions examined.

By examining the beam profiles and radial dependence of grid erosion observed during the ELT [7], it is apparent that the changes in screen grid ion transparency observed during the ELT must be primarily caused by erosive thinning of the screen grid that predominately occurred near the center region of the overall grid area. Therefore, increases in screen grid ion transparency over the life of the thruster at the center gridlet (as observed in the ELT results discussed later) should be much higher than that of the entire beam. As discussed below, further analysis is needed to correlate these magnitudes.

For the profiles in Fig. 2 it is reasonable to use trapezoidal integration between radii 0, 2, 4, 6, 8, 10, and 13 cm to determine the backstreaming limit for the entire beam. Using this technique for ELT profiles at TH15 and TH9 the electron backstreaming limit was very near experimentally determined values as shown in Table 1. Maximum, mean, and minimum values for the $|V_{ebs}|$ values calculated by the model are due to the uncertainty in grid gap as discussed in the previous section and reported in [9]. By examining the details of the relative level of electron backstreaming over the radial extent of the grids, it was found that over 99% of the backstreaming current occurs inside of $r = 6$ cm of the over 28 cm diameter NSTAR grids. For these profiles it was also found that $f_{ebs} \approx 10\%$ for the center hole when $f_{ebs} = 1\%$ for the entire beam. Therefore, an $f_{ebs} \approx 10\%$ for the center hole was used in the following analysis as the condition where the electron backstreaming limit is reached [6].

C. Electron Backstreaming Sensitivities and Comparisons with ELT Data

As discussed later in this section, during full power (TH15) operation of the NSTAR thruster in the ELT the electron

Table 1 Calculated electron backstreaming limit at ELT beginning-of-life

EBS limit $\lvert V_{ebs}\rvert$	Measured, V	Calculated, V		
		Minimum	Maximum	Mean
TH15	150	142	148	145
TH9	130	126	135	132

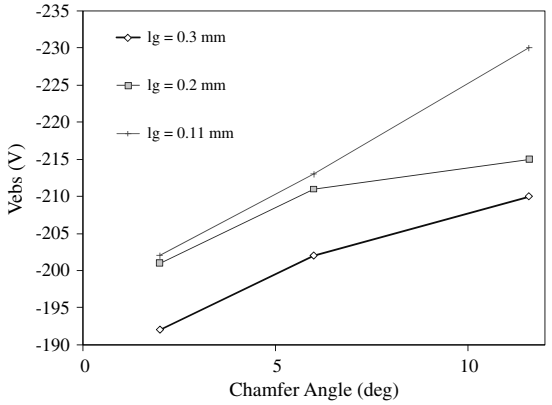

Fig. 4 Electron backstreaming limit vs chamfer angle at grid gaps (lg) of 0.3, 0.2, and 0.11 mm. The grid transparency was constant for a given grid spacing regardless of chamfer angle (i.e., the grid transparency is 87.5 for $l_g = 0.30$ mm, 91.2 for $l_g = 0.20$ mm, and 93.2 for $l_g = 0.11$ mm).

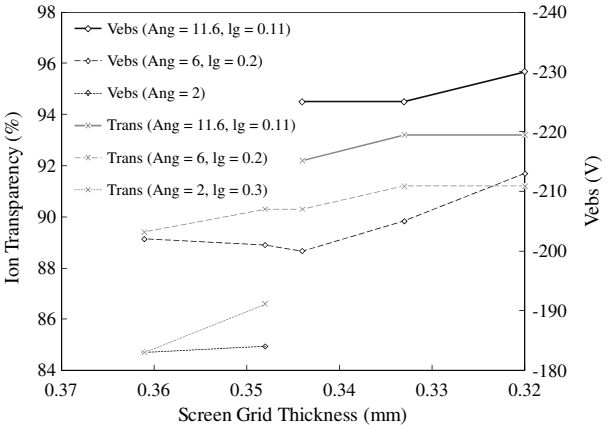

Fig. 6 Electron backstreaming limit (Vebs) and ion transparency (Trans) variation with screen grid thickness for different combinations of chamfer angle (Ang) and grid spacing lg. (Note: transparency change is for center hole only.)

backstreaming limit and the screen grid ion transparency rose dramatically. Before comparing with these observations, it is important to understand the general dependence of electron backstreaming on chamfer angle of the downstream end of the accelerator grid, grid spacing, and screen grid thickness. The effect of these parameters (i.e., chamfer angle, grid spacing, and screen grid thickness) on screen grid ion transparency for the center hole is also be examined to help determine what combination of effects led to the electron backstreaming trends observed during the ELT.

The erosion results for the center hole from [6] suggests that the chamfer angles of the accelerator grid grows from about 2–6 deg during test segment 4, and from about 6–11.6 deg during test segment 6. Examining the electron backstreaming limit V_{ebs} for these chamfer angles at grid spacings of 0.30, 0.20, and 0.11 mm for the center hole (at a nominal end-of-life grid thickness of 0.32 mm and accelerator gridlet diameter of 1.410 mm) reveals a general increase in $|V_{\text{ebs}}|$ with increasing chamfer angle as shown in Fig. 4. The grid transparency to ions for the center hole for the cases examined was constant for a given grid spacing regardless of chamfer angle (i.e., the grid transparency is 87.5 for $l_g = 0.30$ mm, 91.2 for $l_g = 0.20$ mm, and 93.2 for $l_g = 0.11$ mm). From these results it is apparent that increasing chamfer angle contributes to the change in backstreaming limit observed in the ELT but does not explain the rise in ion transparency.

If these results are plotted as a function of grid spacing an increase in both transparency and $|V_{\text{ebs}}|$ is evident; however the change in V_{ebs} is not sufficiently steep to match the ELT results (Fig. 5). This suggests that grid gap change and chamfering work together to increase the electron backstreaming limit. The transparency change is for the center hole only since the intermediate erosion estimates from [6] are only for the center hole.

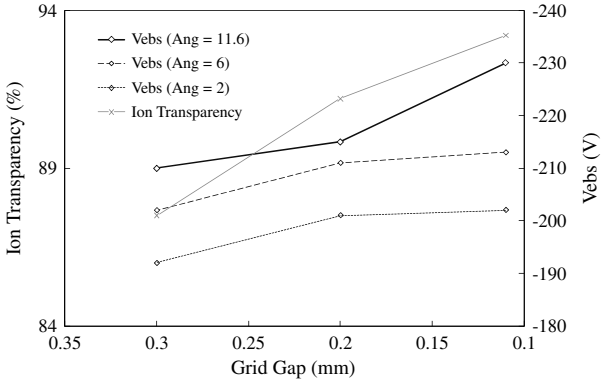

Fig. 5 Electron backstreaming limit V_{ebs} and ion transparency versus grid gap for Chamfer angles (Ang) of 2, 6, and 11.6°. (Note: transparency change is for center hole only.)

Because the erosion profiles do not include effects of redeposition, the variation of screen grid thickness was simply taken as proportional to the propellant throughput, as done in [1]. Using this method, the screen grid thicknesses plotted in Fig. 6 correspond to the test segments as shown on the top axis of the graph. The results for ion transparency and electron backstreaming limit in Fig. 6 show that decreasing screen thickness generally causes both the magnitude of V_{ebs} and screen grid transparency to increase; however, the change in V_{ebs} is not nearly enough to explain the trends seen from the ELT

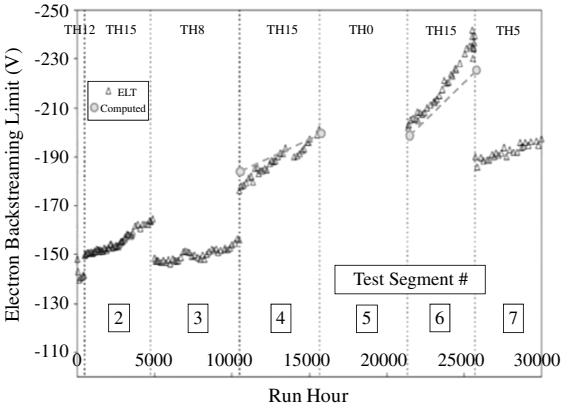

Fig. 7 Measured and computed electron backstreaming limit as a function of time for the ELT.

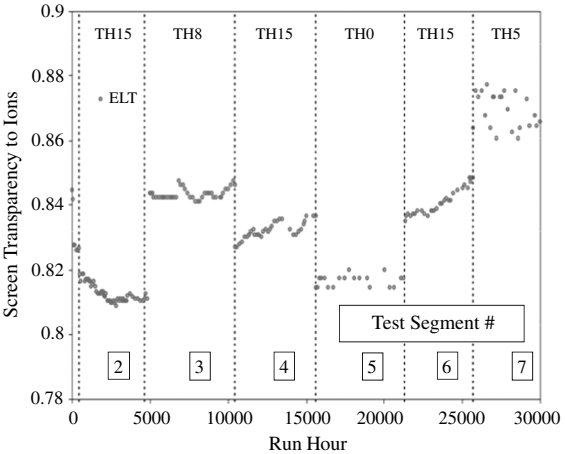

Fig. 8 Screen grid transparency to ions as a function of time during the ELT.

Table 2 Assumed center hole characteristics for the computational results shown in Fig. 7

Time	Chamfer angle, °	Grid spacing, mm	Screen grid thickness, mm
Beginning of test segment 4	2.0	0.3	0.361
End of test segment 4	6.0	0.2	0.348
Beginning of test segment 6	6.0	0.2	0.344
End of test segment 6	11.6	0.11	0.333

(Fig. 7). The screen grid transparency for the center hole due to screen grid erosion is of the same order as that of the entire beam from the ELT results (Fig. 8). However, as mentioned earlier, the required change in screen grid transparency near the center of the grid, where the current density is much higher, should be much greater than the change in transparency for the entire grid.

Combining the effects of chamfering, grid spacing, and screen thickness yields the comparison with ELT data shown in Fig. 7. The computed values assume the conditions for the beginning and end of test segments 4 and 6 for the center gridlet shown in Table 2. The trends in screen grid transparency from the computational results agree with the values shown in Fig. 8; however, additional work is needed to correlate the screen grid transparency values for the center hole with the ELT data for the entire beam.

IV. Conclusions

The technique presented herein for calculating electron backstreaming reveals important aspects of electron backstreaming phenomena for individual beamlets, across the thruster beam, and throughout thruster life. For individual beamlets it was found that over 99% of the electron backstreaming occurs in a small area at the center of the beamlet that is less than 20% the area of the beamlet at the potential barrier established by the accelerator grid. For the 28 cm diameter NSTAR grid, it was found that over 99% of the backstreaming current occurs inside of $r = 6$ cm.

Initial validation against ELT data shows that the technique provides the correct behavior and magnitude of electron backstreaming for the grid geometries and assumptions use herein. From the sensitivity analyses it is apparent that accelerator grid chamfering contributes significantly to the rise in $|V_{\text{ebs}}|$ observed in the ELT but does not explain the rise in ion transparency. Grid gap change also contributes to $|V_{\text{ebs}}|$ rise and large rises in ion transparency with thruster life. Screen grid erosion contributes generally to rises in $|V_{\text{ebs}}|$ and ion transparency, but for the assumptions used herein, it appears to not have as much of an effect as chamfering or grid gap change. Overall, it is apparent that accelerator grid chamfering, grid gap change, and screen grid erosion are important to the increase in electron backstreaming observed during the ELT; while gap change and screen grid erosion contribute to grid transparency change. However, because many of the parameters used herein are uncertain, it is important to perform additional validation and analysis of this technique and its sensitivity to the many inputs to this problem. For example, because this tool is intended to estimate thruster life it is important to rigorously propagate the error associated with the inputs to provide probabilistic failure analysis, similar to that performed in [1].

Acknowledgment

The research described in this paper was carried out by the Jet Propulsion Laboratory, California Institute of Technology, under contract with the National Aeronautics and Space Administration.

References

[1] Brophy, J. R., "Propellant Throughput Capability of the DAWN Ion Thrusters," IEPC Paper 2007-279, Sept. 2007.

[2] Kaufman, H. R., "Technology of Electron-Bombardment Ion Thrusters," in *Advances in Electronics and Electron Physics*, Vol. 36, edited by L. Marton, Academic Press, New York, 1974.

[3] Nakano, M., and Arakawa, Y., "Ion Thruster Lifetime Estimation and Modeling using Computer Simulation," IEPC Paper 99-145, Sept. 1999.

[4] Nakano, M., "A Grid Lifetime Model for a 3-Grid Ion Engine," IEPC Paper 01-84, Oct. 2001.

[5] Williams, J. D., Goebel, D. M., and Wilbur, P. J., "Analytical Model of Electron Backstreaming for Ion Thrusters," AIAA Paper 4560-2003, July 2003.

[6] Wirz, R. E., Anderson, J. R., Katz, I., and Goebel, D. M., "Time Dependent Erosion of Ion Optics," AIAA Paper 4529-2008, July 2008.

[7] Anderson, J. R., et al., "Post-Test Analysis of the Deep Space One Spare Flight Thruster Ion Optics," AIAA Paper 3610-2004, July 2004.

[8] Wirz, R. E., "Discharge Plasma Processes of Ring-Cusp Ion Thrusters," Ph.D. Dissertation, California Institute of Technology, Pasadena, CA, 2005.

[9] Diaz, E. M., and Soulas, G. C., "Grid Gap Measurement for an NSTAR Ion Thruster," NASA TM-2006-214249; also IEPC Paper 2005-244, Nov. 2005.

[10] Patterson, M. J., Haag, T. W., Rawlin, V. K., Kussmaul, M. T., "NASA 30 cm Ion Thruster Development Status," AIAA Paper 94-2849, June 1994.

[11] Brophy, J. R., Katz, I., Polk, J., and Anderson, J. R., "Numerical Simulations of Ion Thruster Accelerator Grid Erosion," AIAA Paper 4261-2002, July 2002.

J. Blandino
Associate Editor